Supplementary Information

Flower-like manganese and phosphorus co-doped MoS$_2$ with high 1T phase content as supercapacitor electrode material

Yunan Li,[*ab] Xiaotian Wang,[a] Jiayin Meng,[a] Meng Song,[a] Mingli Jiao,[a] Qi Qin,[*a] and Liwei Mi[*b]

[a]School of Materials and Chemical Engineering, Zhongyuan University of Technology, Zhengzhou 450007, China

[b]Center for Advanced Materials Research, Henan Key Laboratory of Functional Salt Materials, Zhongyuan University of Technology, Zhengzhou 450007, China

* Corresponding authors.

E-mail addresses: yunanli@zut.edu.cn (Y. Li), qq@zut.edu.cn (Q. Qin), mlwzzu@163.com (L. Mi).

1. Experimental section

1.1. Preparation of the samples

$MnP-MoS_2$ was synthesized by one-step hydrothermal reaction. Typically, 1 mmol ammonium molybdate tetrahydrate (($NH_4)_6Mo_7O_{24}\cdot4H_2O$, 1236 mg), 30 mmol thiourea (($NH_2)_2CS$, 2284 mg), 1.75 mmol manganese chloride tetrahydrate ($MnCl_2\cdot4H_2O$, 346 mg) and 2 mmol sodium hypophosphite (NaH_2PO_2, 176 mg) were dissolved into 20 mL of water under magnetic stirring for 30 min. The precursor solution was then transferred into a 25 mL Teflon-lined stainless-steel autoclave and kept at 180 °C for 24 h. After cooled down naturally to room temperature, the resultant precipitate was collected by centrifugation, washed with water and absolute ethanol several times, respectively, and

finally dried at 60 °C under vacuum. The obtained sample was denoted as $MnP-MoS_2$. Keeping other reaction conditions unchanged, when the amount of NaH_2PO_2 added was respectively 1 mmol and 3 mmol, the obtained sample was denoted as $MnP-MoS_2$-1, and $MnP-MoS_2$-2, respectively. For comparison, $Mn-MoS_2$ was prepared by following the same procedure without adding NaH_2PO_2. Pure MoS_2 was prepared by following the same procedure without adding $MnCl_2\cdot4H_2O$ and NaH_2PO_2.

1.2. Characterization

The morphologies of the samples were examined by a scanning electron microscope (SEM, ZEISS Sigma 300) and a transmission electron microscope (TEM, JEOL JEM-F200). The structure of the samples was characterized by an X-ray diffractometer (XRD; Ultima-IV) with Cu Kα radiation (λ = 0.15141 nm). X-ray photoelectron spectroscopy (XPS, Thermo Scientific K-Alpha) was measured with a monochromatic Al Kα X-ray source (hv = 1486.6 eV). The specific surface area and pore size distribution was derived from nitrogen adsorption/desorption isotherms (Micromeritics ASAP 2460) at 77 K using the Brunauer-Emmett-Teller (BET) method and Barrett-Joyner-Halenda (BJH) model, respectively.

1.3. Electrochemical measurements

All the electrochemical tests were investigated using 2 M KOH as the electrolyte. The working electrode was prepared by mixing the obtained sample (MnP-MoS$_2$, Mn-MoS$_2$ and MoS$_2$) as the active material, polyvinylidene fluoride as the binder and acetylene black as the conductive agent with a weight ratio of 8:1:1 in N-methyl-2-pyrrolidone solvent. Then the slurry was spread on foam nickel, dried overnight at the temperature of 80 °C. Finally, a 10 MPa pressure was applied on the electrode. The active material mass for each electrode was about 2~3 mg cm^{-2}. For three-electrode system, Pt foil and Hg/HgO electrode was used as the counter electrode and the reference electrode, respectively. A two-electrode system was utilized to investigated the electrochemical behavior of ASC. To assemble the ASC device, MnP-MoS$_2$ and AC was used as positive electrode and negative electrode, respectively. The mass of AC was determined by the equation 1.[S1]

$$\frac{m_+}{m_-} = \frac{C_- \times \Delta V_-}{C_+ \times \Delta V_+} \tag{1}$$

Where m (g) is the mass of active material, C (F g^{-1}) refers to the specific capacitance, ΔV (V) represents the voltage range.

Cyclic voltammetry (CV), galvanostatic charge-discharge (GCD) and electrochemical impedance spectroscopy (EIS, frequency: 0.1 Hz–100 kHz) curves were obtained by using a CHI 660E electrochemical workstation at room temperature. The specific capacitance was calculated according to the GCD curves by using the equation 2:

$$C = \frac{I \Delta t}{m \Delta V} \tag{2}$$

Where C represents the specific capacitance (F g^{-1}), I (A) refers to the discharge current, ΔV (V) represents the potential change within the discharge time Δt (s), m (g) corresponds to the mass of active material in three-electrode system and total mass of active material in two-electrode system.

The energy density E (W h kg^{-1}) and power density P (W kg^{-1}) of the ASC device in two-electrode were calculated according to equations 3 and 4:

$$E = \frac{1}{2}C\Delta V^2 \times \frac{1}{3.6} \qquad (3)$$

$$P = \frac{3600E}{\Delta t} \qquad (4)$$

Where C (F g^{-1}) is the specific capacitance of the ASC device, ΔV (V) represents the potential change within the discharge time Δt (s).

2. Figures
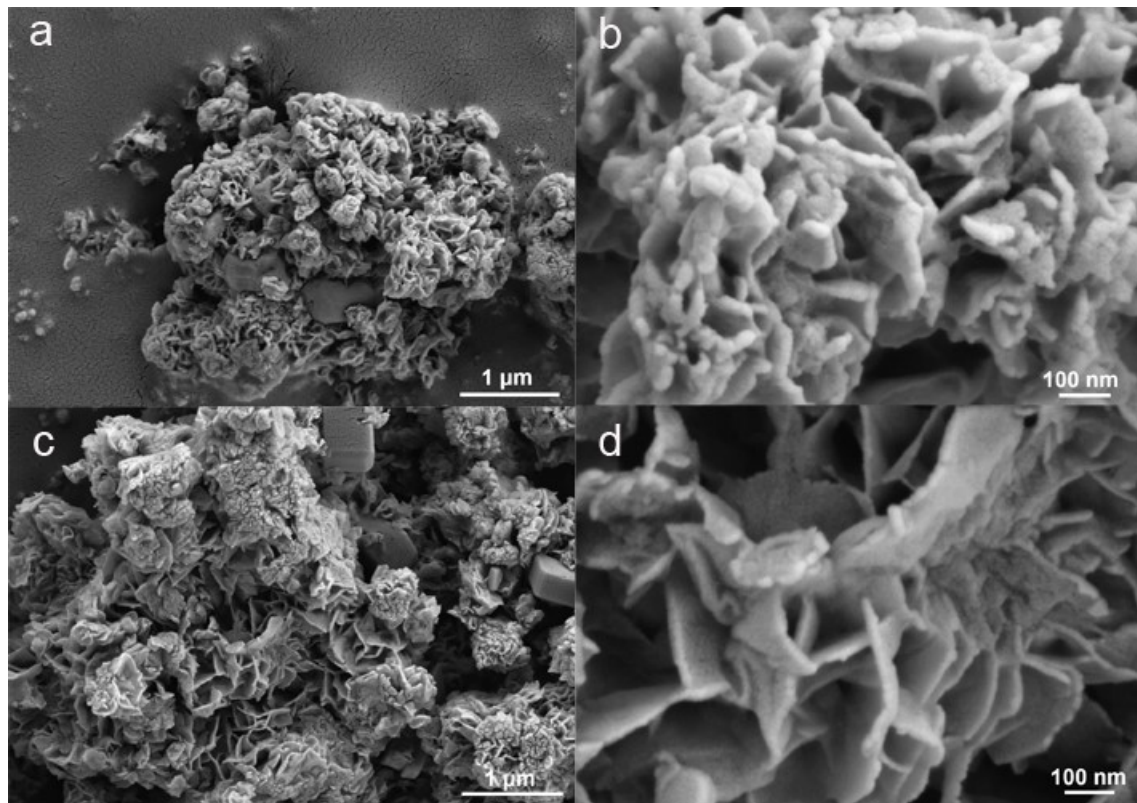
Fig. S1 SEM images of (a, b) Mn-MoS$_2$ and (c, d) MoS$_2$.
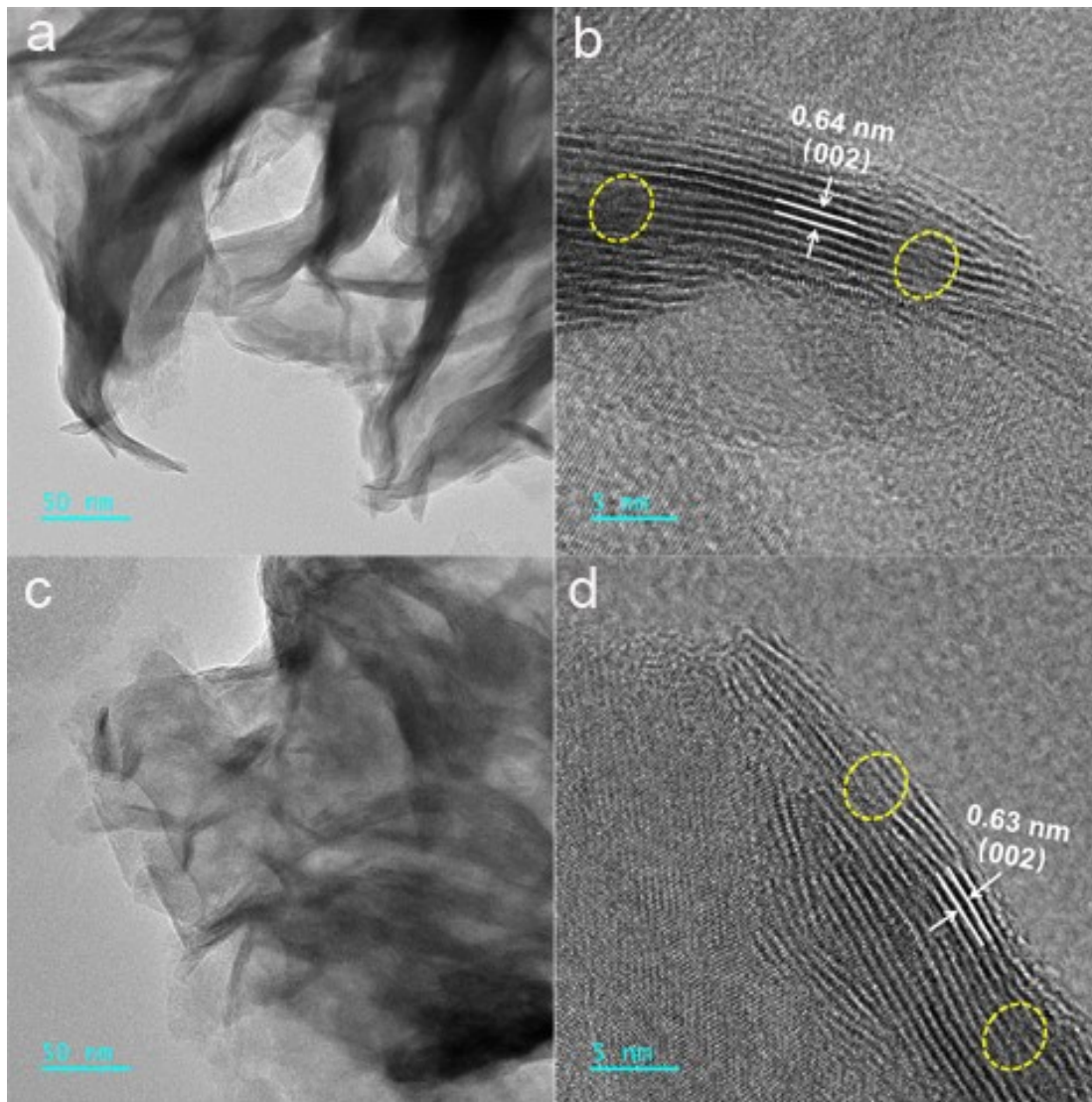
Fig. S2 TEM and HRTEM images of (a, b) Mn-MoS$_2$ and (c, d) MoS$_2$.
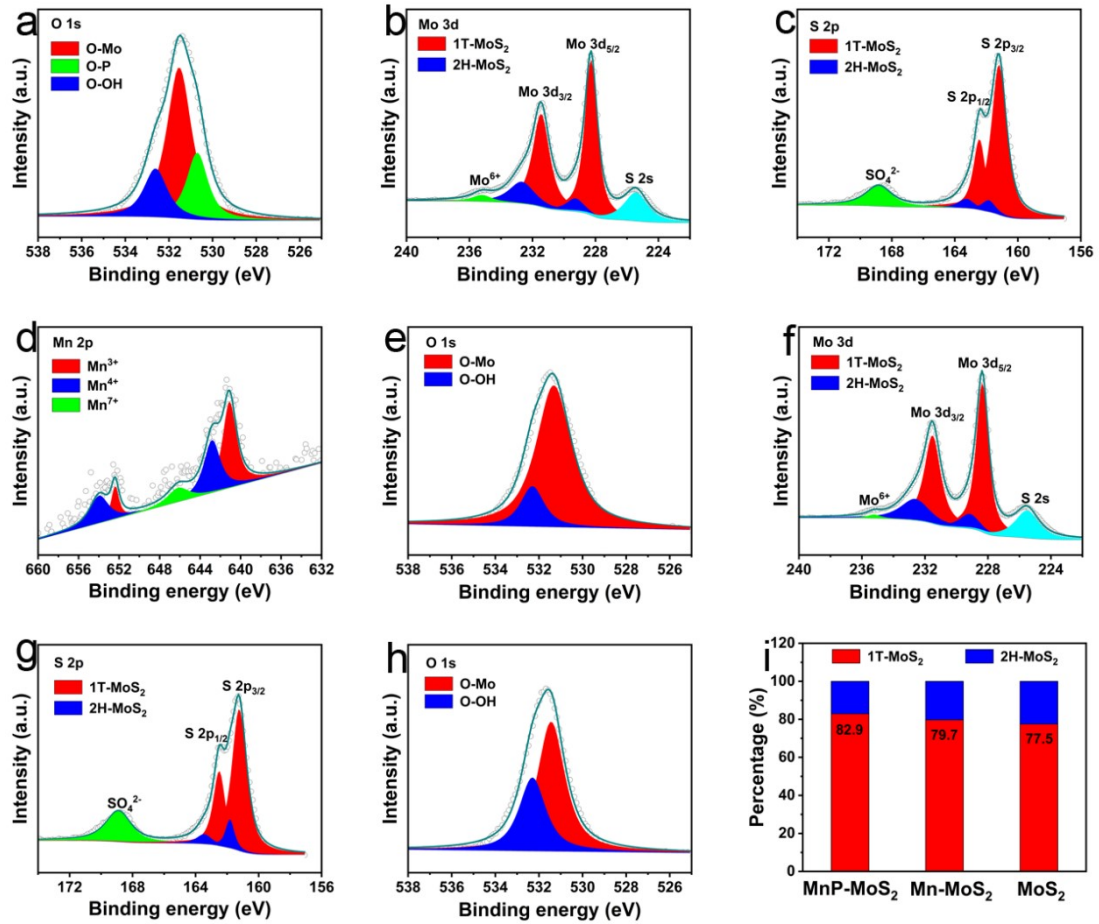
Fig. S3 (a) The high-resolution O 1s spectrum of MnP-MoS$_2$; The high-resolution (b) Mo 3d, (c) S 2p, (d) Mn 2p, and (e) O 1s spectrum of Mn-MoS$_2$; The high-resolution (f) Mo 3d, (g) S 2p, and (h) O 1s spectrum of MoS$_2$; (i) The phase percentage of MoS$_2$ calculated according to the integral area of the Mo 3d spectrum.
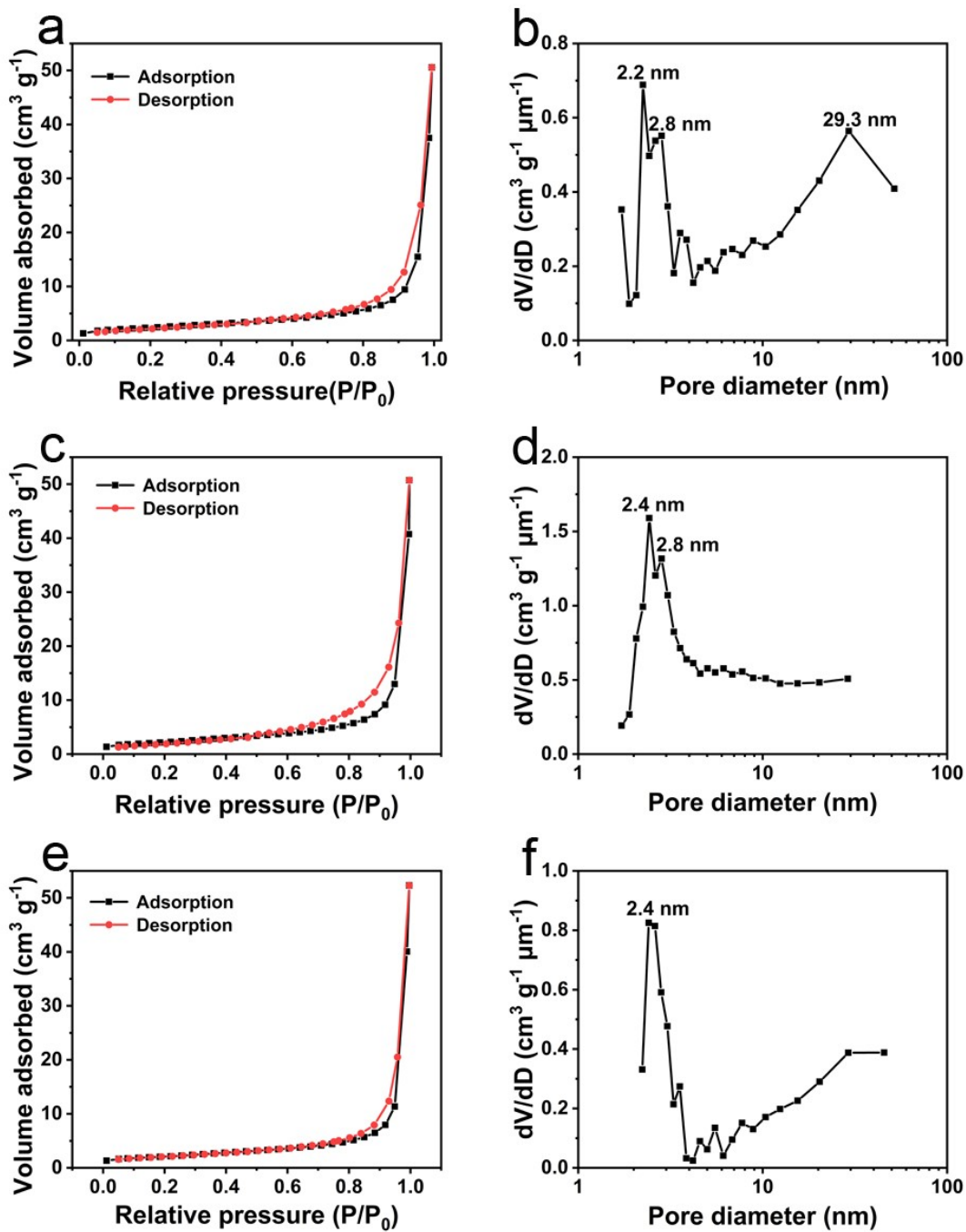
Fig. S4 (a) Nitrogen adsorption-desorption isotherm and (d) Pore size distribution of MnP-MoS$_2$; (b) Nitrogen adsorption-desorption isotherm and (e) Pore size distribution of Mn-MoS$_2$; (c) Nitrogen adsorption-desorption isotherm and (f) Pore size distribution of MoS$_2$.
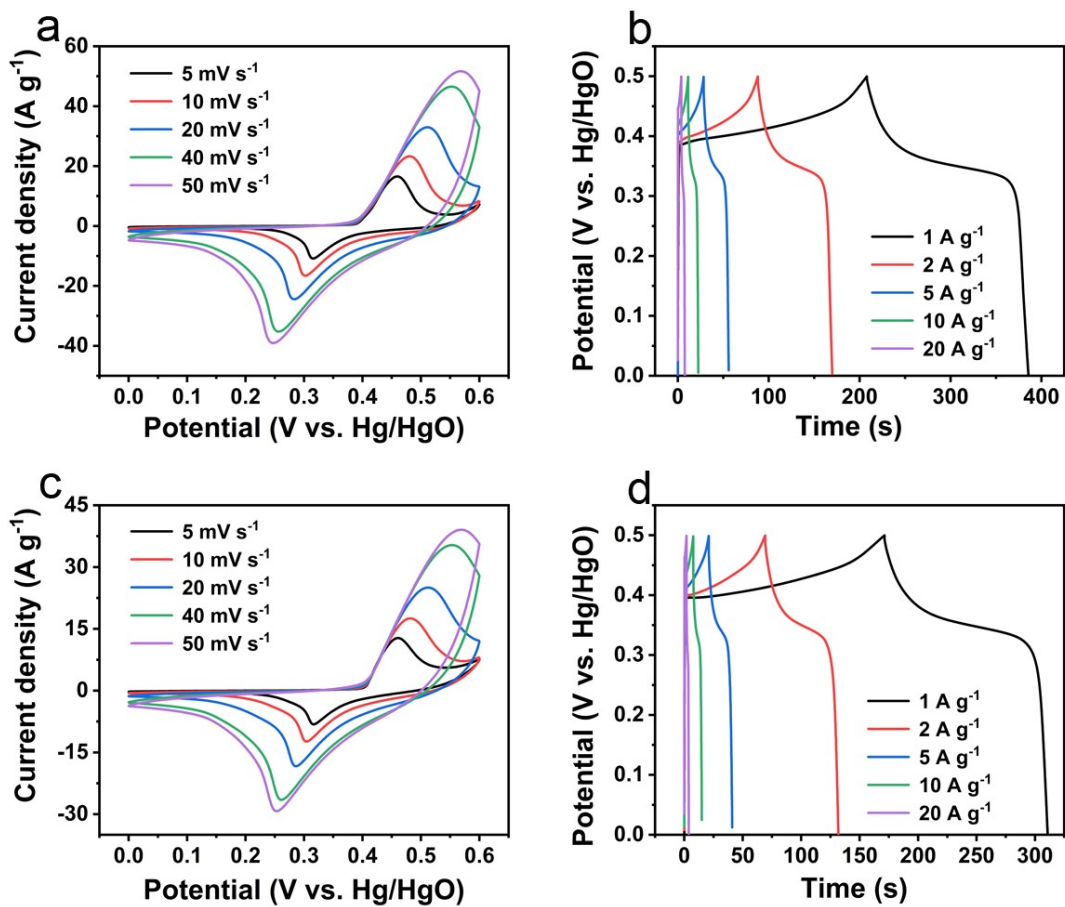
Fig. S5 Electrochemical performance of Mn-MoS$_2$ and MoS$_2$ in three-electrode system. CV curves: (a) Mn-MoS$_2$ and (c) MoS$_2$; GCD curves: (b) Mn-MoS$_2$ and (d) MoS$_2$.
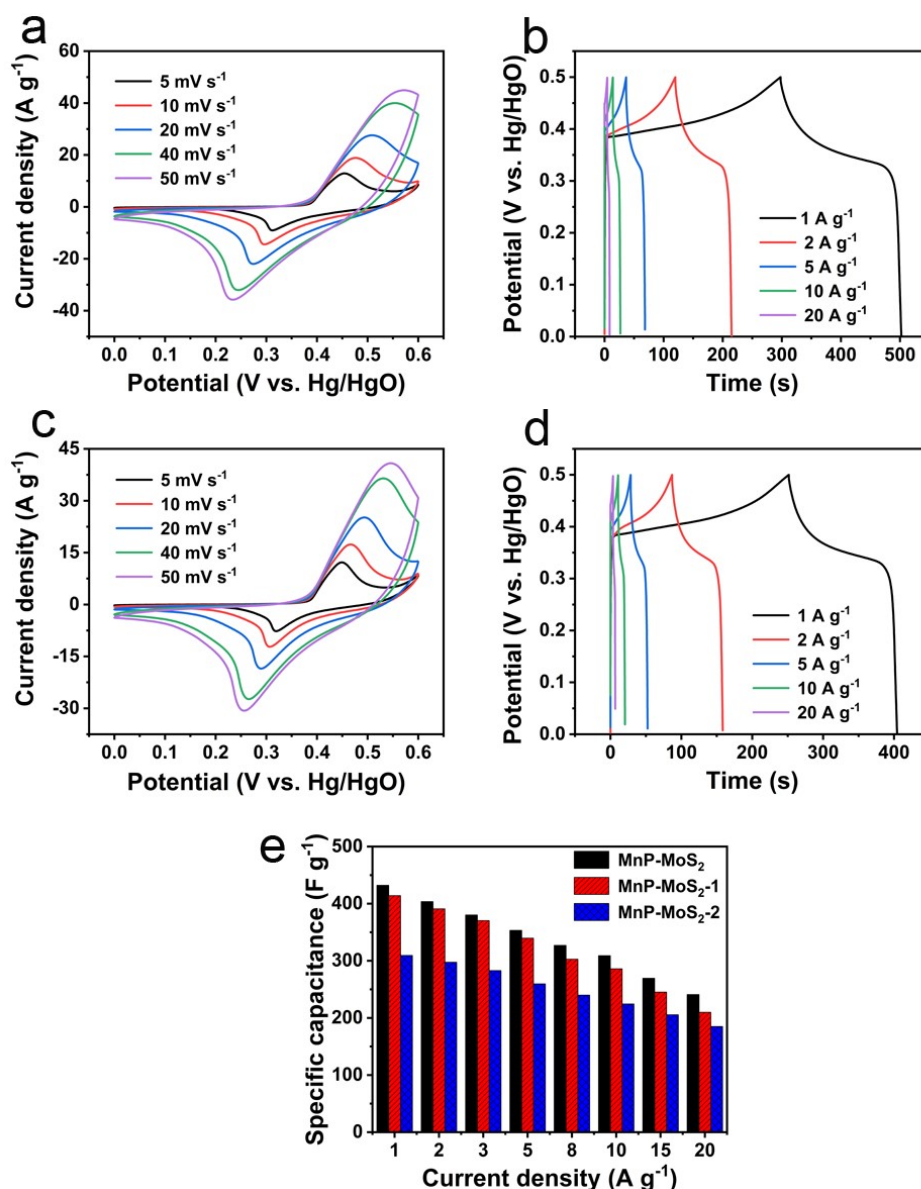
Fig. S6 (a) CV and (b) GCD curves of MnP-MoS$_2$-1; (c) CV and (d) GCD curves of MnP-MoS$_2$-2; (e) Specific capacitance curves of MnP-MoS$_2$, MnP-MoS$_2$-1 and MnP-MoS$_2$-2.

The CV and GCD curves of MnP-MoS$_2$-1 and MnP-MoS$_2$-2 show similar trendy with MnP-MoS$_2$. MnP-MoS$_2$ exhibits a maximum specific capacitance of 432.3 F g^{-1} at 1 A g^{-1}, and 241.0 F g^{-1} at 20 A g^{-1}. In comparison, MnP-MoS$_2$-1 possesses a maximum specific capacitance of 414.1 F g^{-1} at 1 A g^{-1}, and 210.1 F g^{-1} at 20 A g^{-1}. MnP-MoS$_2$-2 displays a maximum specific capacitance of 390.5 F g^{-1} at 1 A g^{-1}, and 185.1 F g^{-1} at 20 A g^{-1}.
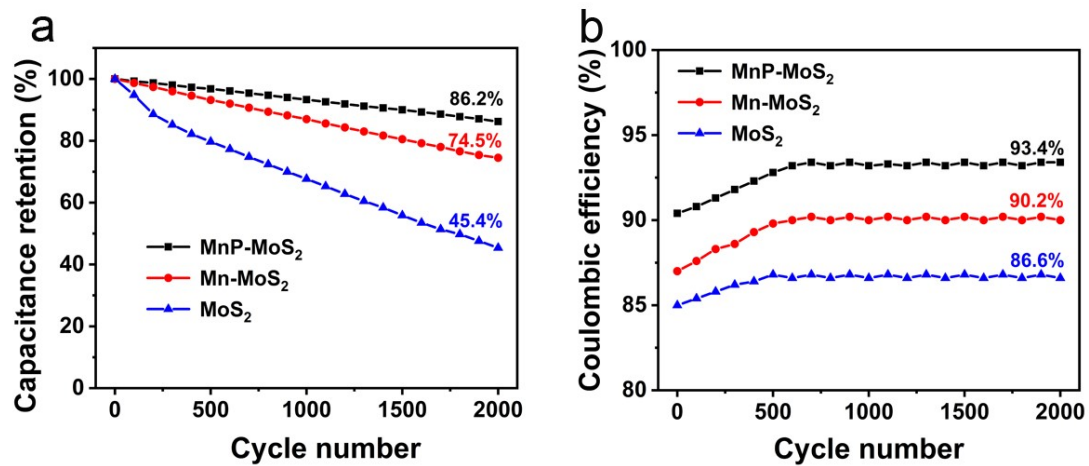
Fig. S7 (a) Cycling stability and (b) coulombic efficiency of MnP-MoS$_2$, Mn-MoS$_2$, and MoS$_2$ after 2000 cycles at a current density of 10 A g^{-1}.
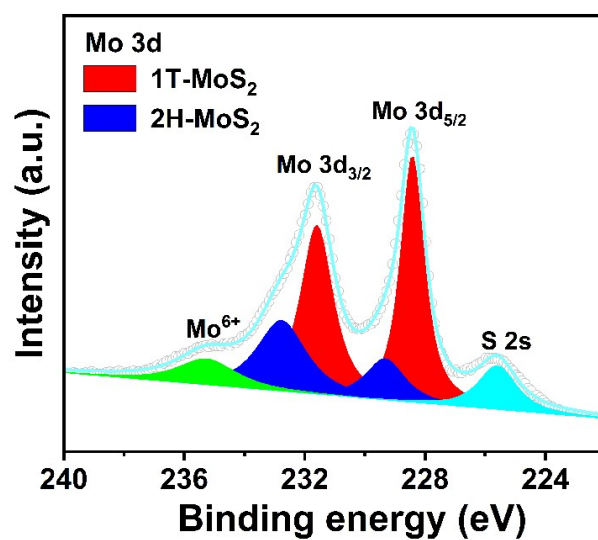
Fig. S8 The high-resolution Mo 3d XPS spectrum of MnP-MoS$_2$ after 2000 cycles at a current density of 10 A g^{-1}.

According to the integral area of the deconvoluted Mo 3d spectrum, the content of 1T phase in MnP-MoS$_2$ after 2000 cycles at a current density of 10 A g^{-1} is about 39.7%.

Table S1 Comparative electrochemical performance of different supercapacitor electrodes in alkaline solution based on heteroatom-doped MoS_2 in literatures with our work.

Electrode material	Electrolyte	Specific capacitance	Rate Capability	Cycling stability
Sr-doped MoS_2[S2]	3 M KOH	489.7 F g^{-1} at 1 A g^{-1}	~300 F g^{-1} at 10 A g^{-1}	62.5% after 2000 cycles
Ni-doped 1T-MoS_2[S3]	1 M KOH	2461.2 F g^{-1} at 1 A g^{-1}	1609.0 F g^{-1} at 5 A g^{-1}	85.67 % after 1000 cycles
Carbon and nitrogen co-doped MoS_2[S4]	6 M KOH	1400 F g^{-1} at 1 A g^{-1}	262 F g^{-1} at 5 A g^{-1}	95 % after 5000 cycles
Cu doped MoS_2[S5]	6 M KOH	353 F g^{-1} at 1 A g^{-1}	267 F g^{-1} at 10 A g^{-1}	94 % after 5000 cycles
Co-decorated MoS_2[S6]	2 M KOH	510 F g^{-1} at 1 A g^{-1}	400 F g^{-1} at 10 A g^{-1}	77.4 % after 5000 cycles
MnP-MoS$_2$ (Our work)	*2 M KOH*	*432.3 F g^{-1} at 1 A g^{-1}*	*309.1 F g^{-1} at 10 A g^{-1}*	*86.2% after 2000 cycles*
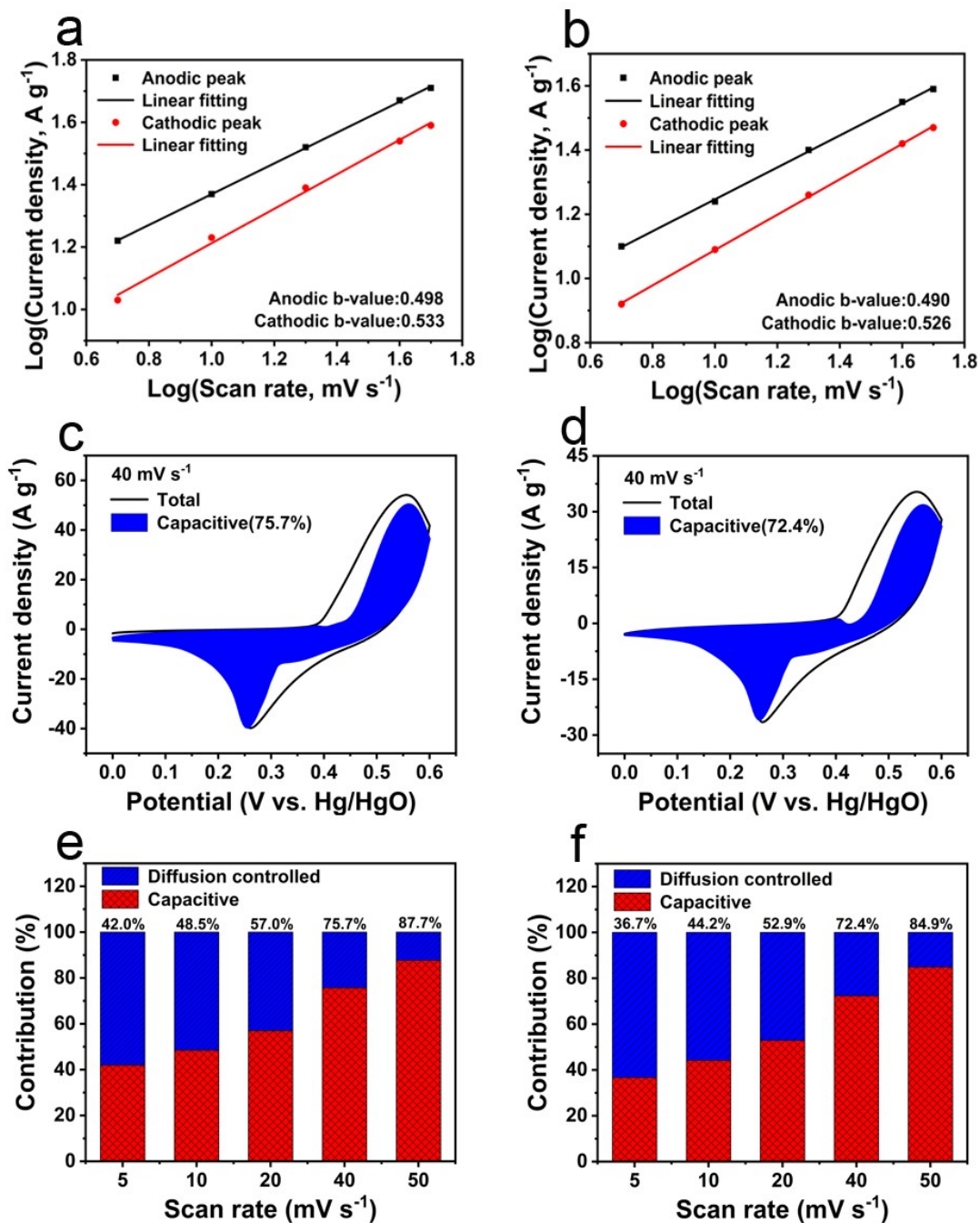
Fig. S9 Electrochemical charge storage mechanism of Mn-MoS$_2$ and MoS$_2$ electrode. Plots of log of anodic and cathodic peak current densities versus log (scan rate): (a) Mn-MoS$_2$ and (b) MoS$_2$; Capacitive and diffusion-controlled charge storage contribution at a scan rate of 40 mV s^{-1}: (c) Mn-MoS$_2$ and (d) MoS$_2$; Capacitive and diffusion-controlled charge storage contribution ratios at various scan rates: (e) Mn-MoS$_2$ and (f) MoS$_2$.
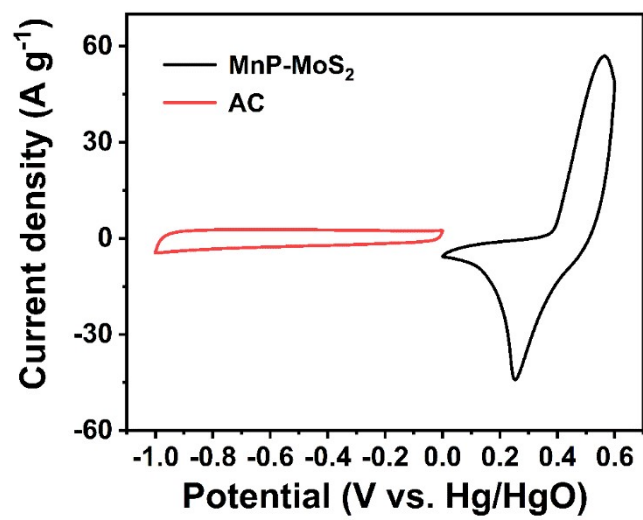
Fig. S10 Comparative CV curves of MnP-MoS$_2$ and AC at a scan rate of 50 mV s^{-1}.

References

S1   Z. Tang, J. Dai, W. Wei, Z. Gao, Z. Liang, C. Wu, B. Zeng, Y. Xu, G. Chen, W. Luo, C. Yuan and L. Dai, *Adv. Sci.*, 2022, **9**, 2201685.

S2   T. K. Selvam, K. Silambarasan, K. Prakash, J. Archana, S. Harish, A. M. F. Benial and T. Mathavan, *J. Mater. Sci.: Mater. Electron.*, 2023, **34**, 345.

S3   Z. Wang, J. Wang, F. Wang, X. Zhang, X. He, S. Liu, Z. Zhang, Z. Zhang and X. Wang, *J. Alloy. Compd.*, 2023, **947**, 169505.

S4   M. G. Fayed, S. Y. Attia, Y. F. Barakat, E. E. El-Shereafy, M. M. Rashad and S. G. Mohamed, *Sustain. Mater. Techno.*, 2021, **29**, e00306.

S5   D. Vikraman, S. Hussain, K. Karuppasamy, A. Kathalingam, E.-B. Jo, A. Sanmugam, J. Jung and H.-S. Kim, *J. Alloy. Compd.*, 2022, **893**, 162271.

S6   A. Sun, L. Xie, D. Wang and Z. Wu, *Ceram. Int.*, 2018, **44**, 13434-13438.